AGU PUBLICATIONS

JGR

Journal of Geophysical Research: Space Physics

RESEARCH ARTICLE
10.1002/2014JA020453

Key Point:
- *X* line poleward of the cusp and *x* line retreat speed measured lead to secondary island

Correspondence to:
F. D. Wilder,
Frederick.Wilder@lasp.colorado.edu

Citation:
Wilder, F. D., S. Eriksson, K. J. Trattner, P. A. Cassak, S. A. Fuselier, and B. Lybekk (2014), Observation of a retreating *x* line and magnetic islands poleward of the cusp during northward interplanetary magnetic field conditions, *J. Geophys. Res. Space Physics*, *119*, 9643–9657, doi:10.1002/2014JA020453.

Received 30 JUL 2014
Accepted 5 NOV 2014
Accepted article online 7 NOV 2014
Published online 4 DEC 2014

Observation of a retreating *x* line and magnetic islands poleward of the cusp during northward interplanetary magnetic field conditions

F. D. Wilder[1], S. Eriksson[1], K. J. Trattner[1], P. A. Cassak[2], S. A. Fuselier[3,4], and B. Lybekk[5]

[1]Laboratory of Atmospheric and Space Physics, University of Colorado, Boulder, Colorado, USA, [2]Department of Physics and Astronomy, West Virginia University, Morgantown, West Virginia, USA, [3]Southwest Research Institute, San Antonio, Texas, USA, [4]Department of Physics and Astronomy, University of Texas at San Antonio, San Antonio, Texas, USA, [5]Department of Physics, University of Oslo, Oslo, Norway

Abstract When the interplanetary magnetic field is northward, reconnection occurs in each hemisphere on lobe field lines, poleward of the cusp. We have identified a case where the Cluster spacecraft crossed the magnetopause and encountered a tailward retreating *x* line. The *x* line is identified by the encounter of both a tailward and sunward jet, as well as Hall magnetic field signatures in the out-of-plane direction. Additionally, we find no signatures of electron heating and hypothesize that the spacecraft is too close to the *x* line to observe the accelerated electrons. Using two spacecraft, we are able to resolve the velocity of the structure, which moves near the magnetosheath speed. The speed of the *x* line is also consistent with the asymmetric reconnection theory. To our knowledge, this is the first time the speed of a retreating *x* line has been measured directly. Additionally, we observe ion distribution functions with counterstreaming populations, suggesting that a second *x* line formed sunward of the original one, leading to a magnetic island.

1. Introduction

Magnetic reconnection is a fundamental driver of large-scale plasma convection and energy transport in planetary magnetospheres. At the Earth, it is well understood that under southward interplanetary magnetic field (IMF), magnetic reconnection on the dayside magnetopause near the subsolar point drives large-scale convection that maps to the polar ionosphere [*Dungey*, 1961]. Evidence for reconnection in the form of Alfvénic plasma jets has been observed via in situ measurements in repeated studies over the past several decades [e.g., *Paschmann et al.*, 1979; *Sonnerup et al.*, 1981; *Gosling et al.*, 1991; *Phan et al.*, 2001]. When the IMF is northward, reconnection is more likely to occur at high latitudes, poleward of the magnetospheric cusps [e.g., *Dungey*, 1963; *Crooker*, 1992]. Observations of accelerated plasma jets due to reconnection near the cusp have been observed [*Kessel et al.*, 1996; *Phan et al.*, 2003, 2004] and have been shown to be associated with high-latitude sunward flow channels on open field lines in the polar ionosphere [e.g., *Eriksson et al.*, 2005; *Wilder et al.*, 2011, 2012].

Because the magnetosheath plasma accelerates as it flows over the polar region, magnetic reconnection at high latitudes generally proceeds in the presence of a high-flow shear across the magnetopause [*Gosling et al.*, 1991; *Fuselier et al.*, 2000]. This can have several effects on the behavior of the *x* line. Because reconnection exhausts flow at the local Alfvén speed [e.g., *Sonnerup et al.*, 1990], a super-Alfvénic flow shear across the magnetopause current sheet could cause the *x* line to become unstable. One hypothesis is that when the magnetosheath flow is super-Alfvénic, the *x* line will move at a speed such that in its own frame of reference, the magnetosheath flow will be sub-Alfvénic [*Gosling et al.*, 1991; *Fuselier et al.*, 2000]. On the contrary, if the magnetosheath flow is sub-Alfvénic poleward of the cusp, the *x* line will remain at rest. For example, *Fuselier et al.* [2000] suggested that their observation of the cusp signatures of a steady *x* line during northward IMF was due to sub-Alfvénic magnetosheath flow near the *x* line in the Earth-fixed frame. One consequence of a tailward moving *x* line is the possibility of a second *x* line forming at the original location of the first *x* line. For example, *Hasegawa et al.* [2008] found an event during near-northward IMF where evidence suggested that an active *x* line retreated and a new *x* line formed in its original location, leading to a tailward propagating magnetic island.

In this study, we have identified a high-latitude magnetopause crossing in which two spacecraft from the Cluster mission [*Escoubet et al.*, 2001] flew very close to the *x* line when the IMF was northward. Because the

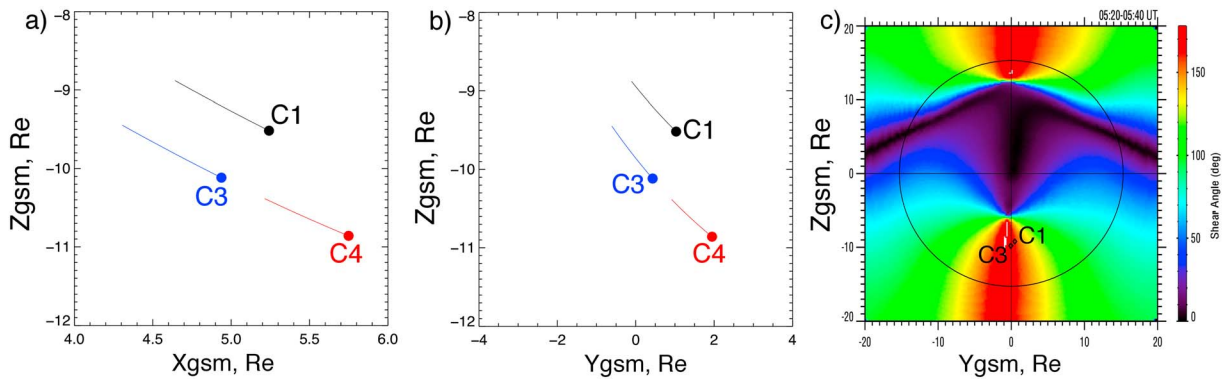

Figure 1. The trajectories of Clusters 1, 3, and 4 in the (a) *X-Z* and (b) YZ_{GSM} planes between 5 and 6 UT on 27 December 2005. Cluster 2 was inside the magnetopause during the entire interval. Additionally, (c) the positions of Clusters 1 and 3 in the YZ_{GSM} plane plotted over the predicted magnetic shear angle on the magnetopause were also shown.

spacecraft were nearly adjacent along the magnetopause surface, we were able to capture the motion of the *x* line and confirm that it moved tailward at a speed that made the magnetosheath flow sub-Alfvénic in the reference frame of the *x* line. We also show that the *x* line speed was consistent with MHD scaling analyses for asymmetric reconnection. Once the *x* line retreated, a secondary *x* line appeared, leading to the formation of a magnetic island.

2. Observations of the Magnetopause Crossing

2.1. Overview

In this study we present a magnetopause crossing in the southern hemisphere by the Cluster spacecraft [*Escoubet et al*., 2001] on 27 December 2005, during northward IMF conditions. The data used will be from the onboard fluxgate magnetometer (FGM) [*Balogh et al*., 2001], the Cluster Ion Spectrometry hot ion analyzer (HIA) [*Rème et al*., 2001], and the Plasma Electron and Current Experiment (PEACE) electrostatic electron analyzer [*Johnstone et al*., 1997]. Because the HIA may not be able to obtain accurate plasma densities in the lobe, we will use plasma density derived from the spacecraft potential measured by the Electric Field and Waves (EFW) suite when the number density is below 0.5 cm^{-3} [*Lybekk et al*., 2012].

Figure 1 shows the trajectory of three of the Cluster spacecraft between 5 and 6 UT on 27 December 2005. Cluster 1 (C1) and Cluster 3 (C3) were closer to the Earth than Cluster 4 (C4) and moving earthward. This study will focus on a magnetopause crossing by C1 and C3. C4, as will be discussed further in section 3, remained in the magnetosheath during the period when C1 and C3 crossed the magnetopause. Cluster 2 was not included in Figure 1 since it crossed the magnetopause at approximately 4:35 UT, almost an hour before C1 and C3. Figure 1c shows the mean location of C1 and C3 between 5 and 6 UT in the *Y-Z* plane, plotted over the predicted magnetic shear angle at the magnetopause using Wind spacecraft [*Lepping et al*., 1995; *Lin et al*., 1995] data and the methodology outlined by *Fuselier et al*. [2011]. Both spacecraft were in the region of the *Y-Z* plane with the largest magnetic shear, and thus, a magnetopause crossing by either spacecraft is likely to observe a reconnection event.

Figure 2 shows a time series of data between 4:00 and 7:00 UT on 27 December 2005 from C1 and C3. During the first half of the interval, both spacecraft were in the southern hemisphere magnetosheath, as evidenced by the large plasma density and southward/antisunward plasma flows around the magnetosphere. Additionally, HIA energy spectrograms (not shown) were consistent with magnetosheath plasma. During this time, the magnetosheath magnetic field, on average, had sunward and northward orientations.

Near 5:30 UT, the magnetic field observed by both spacecraft changed direction, with a significant rotation in the Z_{GSM} direction and less so in the X_{GSM} direction, consistent with the crossing of a current sheet at the magnetopause. At this time, the ion number density also dramatically decreased from approximately 60 cm^{-3} to approximately 0.1 cm^{-3}, and the ion velocity in the X_{GSM} and Z_{GSM} directions changed sign and is accelerated significantly compared to magnetosheath flow. This is consistent with a reconnection exhaust at the magnetopause [e.g., *Eriksson et al*., 2004, and references therein]. After crossing the magnetopause

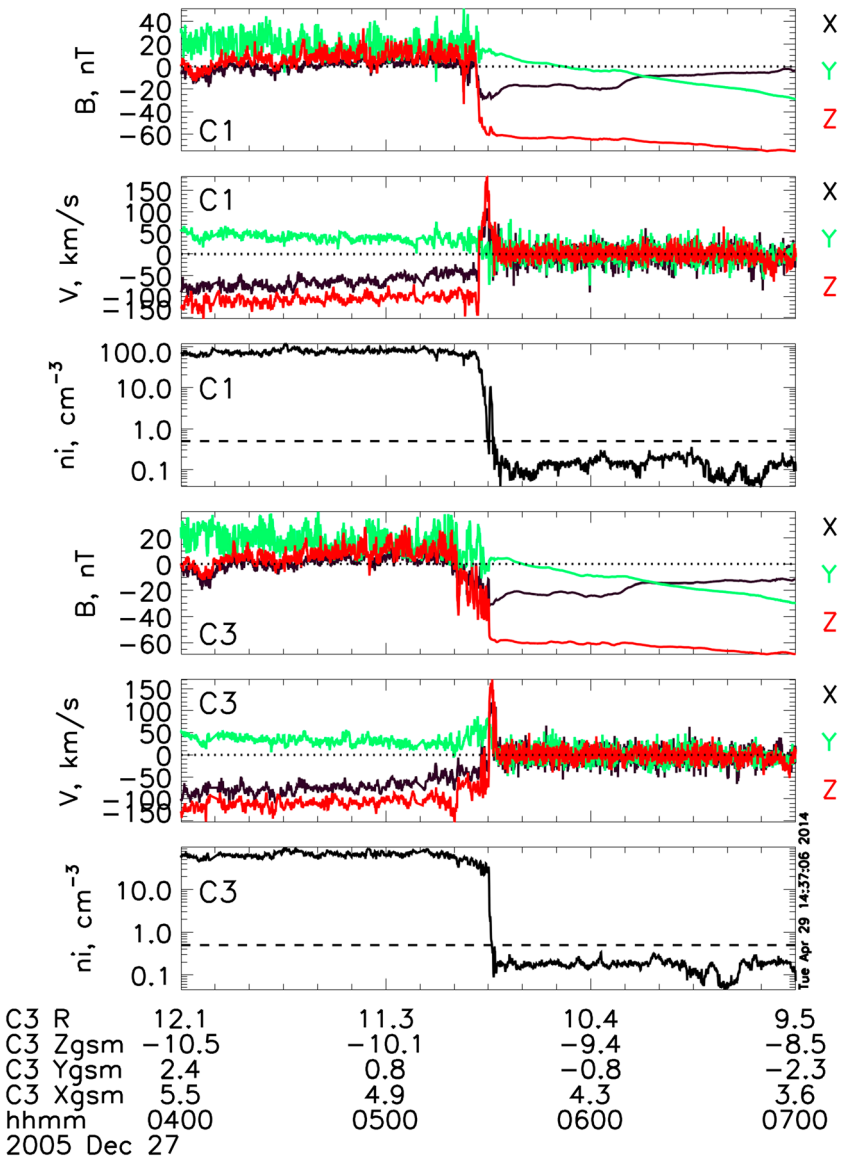

Figure 2. Stackplot of Clusters 1 and 3 data. (top to bottom) Cluster 1 magnetic field, velocity, and hot ion density, followed by Cluster 3 magnetic field, velocity, and hot ion density. The position of Cluster 3 is also given in Earth radius, GSM. All vector quantities are specified in the GSM coordinate system. The dashed black lines in the number density plots indicate the value below which EFW data were used instead of HIA (0.5 cm^{-3}).

current sheet, the spacecraft observe near-zero velocity, steady magnetic field values, and a very low plasma density for the rest of the interval shown, consistent with magnetospheric conditions.

The remainder of this study will focus on the interval in which C1 and C3 observe reconnection exhausts. Because the spacecraft were crossing a current sheet, the magnetic field and velocity data are analyzed in boundary normal coordinates determined by minimum variance analysis (MVA) of the magnetic field [*Sonnerup and Scheible*, 1998]. For C1, we used the interval between 5:25:00 and 5:30:00 UT. The resulting eigenvalues from the MVA analysis are $\lambda_1 = 992.00$, $\lambda_2 = 47.59$, and $\lambda_3 = 5.73$, giving a ratio between the intermediate and minimum eigenvalues of 8.31. This ratio indicates a good determination of the minimum variance direction and therefore a good estimate for the boundary normal direction [*Sonnerup*, 1971; *Sonnerup et al*., 1987; *Phan et al*., 2001]. In this study, the directions $\hat{L}$, $\hat{M}$, and $\hat{N}$ correspond to the directions of maximum, intermediate, and minimum variance, respectively, where $\hat{L} = (0.40, 0.05, 0.92)$, $\hat{M} = (0.09, 0.99, -0.09)$, and $\hat{N} = (-0.91, 0.12, 0.39)$ in the GSM coordinates. For C3, because the spacecraft encounters a

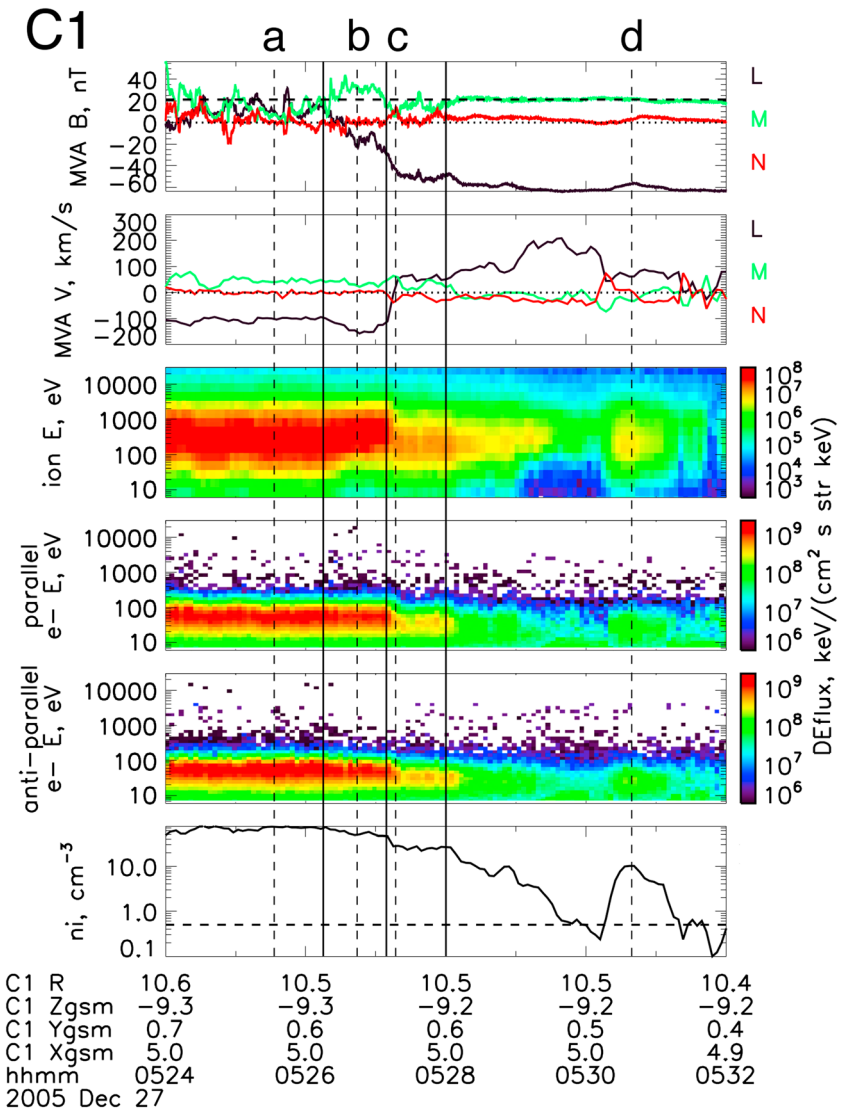

Figure 3. Cluster 1 data during the magnetopause crossing. (top to bottom) Magnetic field data in the "LMN" basis determined through minimum variance analysis (MVA), velocity moments from the HIA in the MVA basis, the spectrogram of ion differential energy flux observed by HIA, spectrograms of differential energy flux measured by PEACE for electrons with parallel and antiparallel streaming, and the ion density determined by both HIA moments and the spacecraft potential. The solid vertical lines indicate three times: when C1 observes a tailward acceleration of plasma from the magnetosheath reference (5:26:15 UT), when C1 observes a sunward acceleration of plasma from the magnetosheath reference (5:27:09 UT), and when C1 no longer sees Hall magnetic field signatures (5:28:00 UT). The vertical dashed lines correspond to times when ion distribution functions from C1 will be shown (see Figure 7). The horizontal dashed line in Figure 3 (top) is the mean guide field (B_M) inside the magnetopause, and the horizontal dashed line in Figure 3 (bottom) represents number density of 0.5 cm^{-3} below which the EFW spacecraft potential provided the density measurements.

complex structure on the magnetopause (see section 3), we were unable to determine a unique MVA coordinate system. For this study, we used the MVA coordinate system from C1 for both spacecraft under the assumption that they are close enough together that the large-scale orientation of the magnetopause current sheet is unchanging.

2.2. Crossing of the *X* Line by Cluster 1

Figure 3 shows data from C1 presented in the MVA coordinates as the spacecraft crossed the magnetopause between 5:24 and 5:32 UT. The three solid vertical lines indicate three time intervals of interest. After the first vertical line, at 5:26:15, C1 passed into a region where the ions were energized compared to the

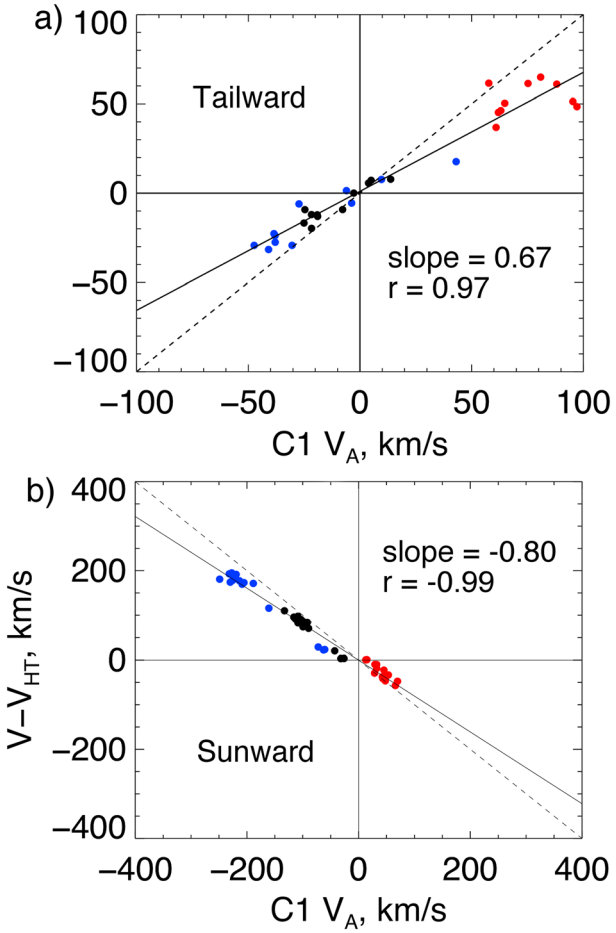

Figure 4. Cluster 1 Walén test for (a) the tailward jet and (b) the sunward jet. The black, red, and blue indicate velocities in the *X*, *Y*, and Z_{GSM} directions.

magnetosheath plasma as the *L* component of the magnetic field rotated from positive to negative. Additionally, there was an enhancement in the *L* component of the velocity in the negative *L* direction, which in the C1 MVA basis is approximately tailward and southward. There was also a positive enhancement in the *M* component of the magnetic field with respect to the background field, given by the dashed horizontal line in Figure 3 (top). These are signatures of observing a tailward directed reconnection exhaust.

The second solid vertical line, at 5:27:09 UT, indicates the point where the *L* component of the plasma velocity returned to its value in the magnetosheath. After this point, the velocity changed direction to sunward and northward flows, the ion fluxes were significantly reduced, and there was a negative reduction in the *M* component of the magnetic field with respect to the background field. These are signatures of crossing a sunward directed reconnection exhaust. The final solid vertical line, at 5:28:00 UT, indicates when the *M* component of the magnetic field returned to the background level.

We can verify whether the two intervals outlined by the vertical black lines are actual crossings of a reconnection exhaust by using a Walén test for the velocity in the jet. This tests for the presence of a rotational discontinuity by examining, quantitatively, whether plasma velocity is Alfvénic in the deHoffmann–Teller frame, as expressed in equation (1) [*Sonnerup et al.*, 1990; *Eriksson et al.*, 2004].

$$V - V_{HT} = \pm V_A = \frac{B_{JET}(1 - \alpha_{JET})}{\sqrt{\mu_0 \rho_0 (1 - \alpha_0)}} \quad (1)$$

Here B_{JET} is the magnetic field vector, ρ is the plasma mass density, and $\alpha = (P_{||} - P_{\perp})\mu_0/B^2$ is the pressure anisotropy term. The subscript "0" refers to the reference parameters measured just outside the reconnection exhaust, determined from averaged values between 5:25:30 and 5:26:00 UT, and the subscript "JET" refers to a time series of values measured throughout the two jet candidate intervals. We used two intervals for the Walén test. For the tailward jet, we used 5:26:15 to 5:27:00 UT, and for the sunward jet, we used 5:27:00 to 5:28:00 UT. V_{HT} is the velocity of the deHoffmann–Teller frame and is determined from a fit to data for each interval using the technique described by *Sonnerup et al.* [1987]. For the tailward jet, $V_{HT} = (-45.02, -33.43, -113.70)$ and had a minimized error of 0.003, and for the sunward jet, with $V_{HT} = (-55.34, 65.35, -139.77)$ km/s in the GSM basis and had a minimized error of 0.081.

Figure 4 shows Walén relation calculated for data points in the tailward jet (Figure 4a) and the sunward jet (Figure 4b). The solid line is a linear fit to the data, and the dashed line is the theoretical relation in equation (1). The calculations were performed under the assumption that the plasma consisted of ionized hydrogen. The slopes of the linear fit for the tailward and sunward jets are 0.67 and −0.80, respectively, and the correlation coefficients between $V - V_{HT}$ and V_A are 0.97 and −0.99, respectively. These values for the slope and the

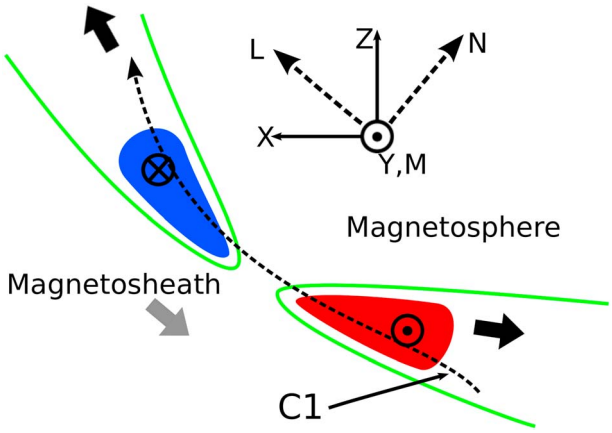

Figure 5. Diagram of Cluster 1 *x* line encounter. The green lines are the magnetic field lines. The black arrows indicate the exhaust directions, and the grey arrow indicates the magnetosheath flow direction. The blue and red regions indicate the location of Hall magnetic field signatures. The dashed line indicates the trajectory of the C1 spacecraft in the rest frame of the *x* line.

correlation coefficients are within the range typically considered to be a good agreement between the data and the Walén relation [*Trenchi et al.*, 2008, and references therein]. The results of the Walén test signify that both the tailward and sunward acceleration intervals are reconnection exhausts.

The fact that C1 observed the reconnection exhaust changing directions suggests that the reconnection *x* line passed near the spacecraft. Additionally, it is likely that C1 passed through the ion diffusion region, as the fluctuations in the *M* component of the magnetic field resemble Hall magnetic fields, which are generated by current loops created due to the ions becoming demagnetized further away from the *x* line than the electrons [*Mozer et al.*, 2008a, *Malakit et al.*, 2010]. The *M* component of the magnetic field deviated from the mean B_M of 20 nT by 7 nT in the tailward jet and −7 nT in the sunward jet. We note that the *N* component was very small, and therefore, it is likely that the spacecraft's crossing was offset from the neutral point where the *N* component would be maximized.

During the interval in Figure 3, C1 was mostly moving earthward, and therefore, to observe both reconnection exhausts, the *x* line would have to have a significant velocity in the *L* direction. Putting all of these together, Figure 5 shows a diagram of the structure C1 that passed through from the reference frame of the assumed moving *x* line. It should be noted that because of the density asymmetry across the magnetopause, it is highly likely that the Hall fields were bipolar and largely influenced by the current loops generated from the incoming magnetosheath plasma which crosses the magnetopause [e.g., *Mozer et al.*, 2008a, 2008b]. These correspond to the observed perturbations in the *M* component of the magnetic field observed by Cluster, which are shown in Figure 3 and conceptualized in Figure 5. This might appear counterintuitive if one assumes that the Hall fields that generated due to incoming magnetosheath plasma would only appear on the magnetosheath side of the current sheet (e.g., the positive B_L region), but recent simulation studies suggest that this is not the case. *Malakit et al.* [2010] performed particle-in-cell simulations of asymmetric reconnection and found that the Hall fields dominated by the current loops set up by the incoming high-density plasma filled the exhaust near the *x* line and were not confined to the high-density side of the current sheet.

Finally, the fourth and fifth panels from the top of Figure 3 include the electrons with parallel (−45 to 45° pitch angle) and antiparallel (135 to 225° pitch angle) streaming, respectively. Below 200 eV energy, fluxes parallel and antiparallel to the field change from the first vertical dashed line, where they were more symmetric, to a slight preference for more 200 eV electrons parallel to the field at the second vertical dashed line. Given that the magnetic field inside the magnetopause at this point was tailward, "parallel" streaming corresponds to tailward fluxes. Additionally, shortly after the third vertical dashed line, there was a region where antiparallel electrons were favored, which would correspond to sunward fluxes. These directions are consistent with the jet motion.

It is important to note that when C1 entered the reconnection exhaust, no upward shift in the electron distributions was observed, and therefore, there was little evidence for electron heating. An explanation for this may be that C1 was too close to the *x* line, where stored magnetic energy is first converted to particle kinetic energy, and therefore, the effects of the electron heating should have been more easily observed in the exhaust region farther away from the *x* line. This is consistent with a hypothesis given by *Fuselier et al.* [2012], who argued that events at high latitudes where Cluster observed little-to-no electron heating or suprathermal electron activity were events where the spacecraft were likely close to the *x* line.

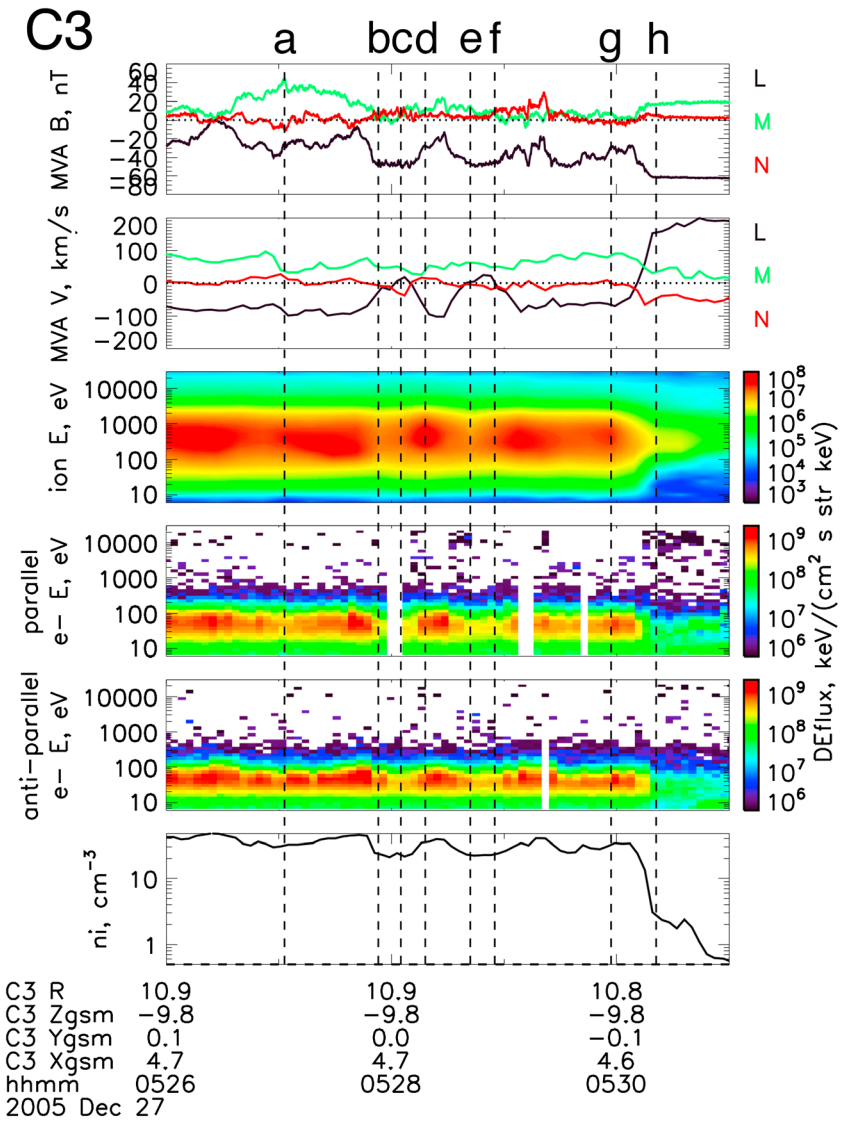

Figure 6. Cluster 3 data at the magnetopause. (top to bottom) Magnetic field data in the LMN basis determined through minimum variance analysis (MVA), velocity moments from the HIA in the MVA basis, the spectrogram of ion differential energy flux measured by HIA, spectrograms of differential energy flux measured by PEACE for electrons with parallel and antiparallel streaming (within 45° of 0° and 180° in pitch angle, respectively), and the ion density determined by both HIA moments and the spacecraft potential. The vertical dashed lines correspond to times when ion distribution functions from C3 will be shown (see Figure 8).

3. Motion of the *X* Line and Magnetic Island Formation

3.1. Ion Distributions and the Speed of the *X* Line Retreat

In the previous section, it was inferred that the *x* line moved tailward and southward past the C1 spacecraft. One advantage to using data from the Cluster mission is its multispacecraft approach. Referring again to Figure 1a, C3 was tailward and southward of C1, and thus, a structure with a tailward and southward velocity should encounter C3 shortly after it is observed by C1. It is worth noting that during this interval, C4 was in the magnetosheath, which will be used to determine if changes in the magnetosheath magnetic field are impacting the structure.

Figure 6 shows time series from C3 between 5:26 and 5:31 UT, where the MVA basis determined from C1 data was used. During this entire interval, C3 was observing a magnetic field vector in the southward and tailward, or the negative *L*, directions. This implies that C3 was already on the magnetospheric side of the

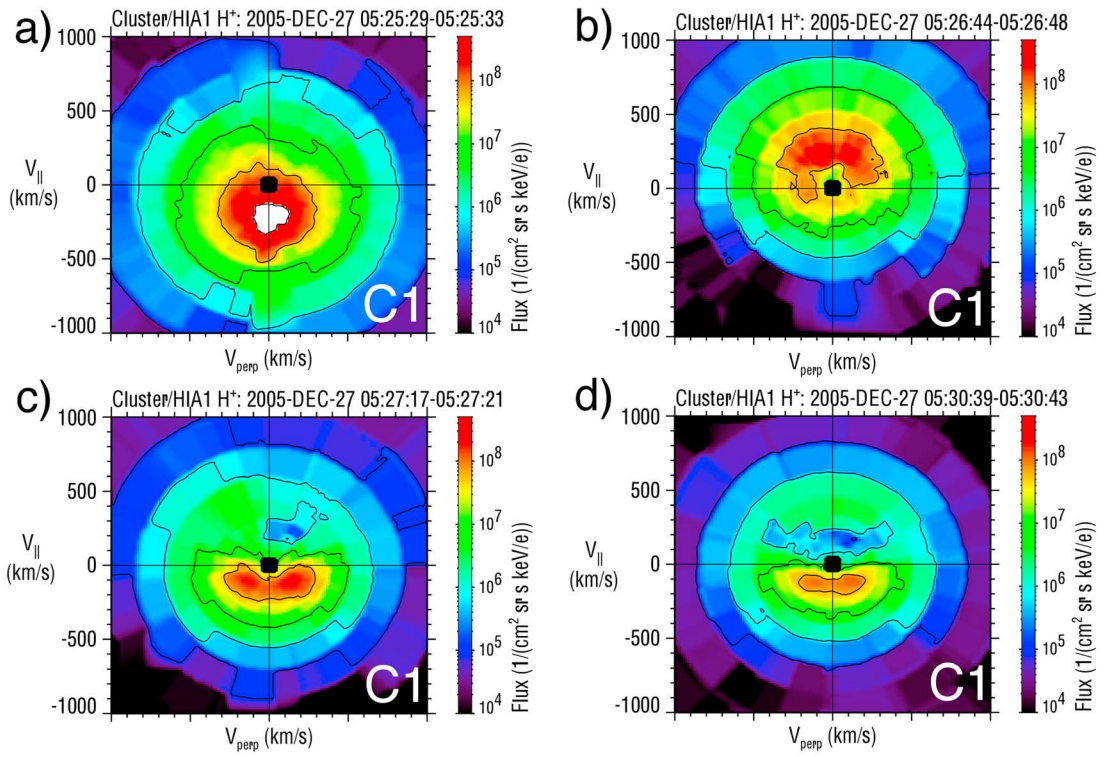

Figure 7. Cluster 1 ion distributions in the *X-Z* plane calculated over 4 s intervals with the start times corresponding to the vertical dashed lines in Figure 2.

magnetopause current sheet. With the flow also being in the negative *L* direction, it is likely that C3 is observing the tailward reconnection exhaust, which we will verify with distribution functions. C3 then proceeded to observe two reversals in flow from tailward to sunward between approximately 5:28 and 5:29 UT before it observed a consistent sunward exhaust beginning at approximately 5:30. Again, in the electron data, no clear evidence of electron heating was observed.

To resolve the motion of the *x* line at the magnetopause, the ion distribution functions (DFs) from which the plasma moments are derived can be used. Figure 7 shows four ion distributions within the *X-Z* plane measured by the HIA instrument on C1, calculated over 4 s intervals with the start times corresponding to the vertical dashed lines in Figure 3. Figure 7a shows a roughly Maxwellian DF with a bulk flow antiparallel to the magnetic field. Comparing with Figure 3, the magnetic field was in the northward/sunward ($B_L > 0$) direction, and C1 was in the magnetosheath, thus, the antiparallel flow is the southward/antisunward flow of the magnetosheath plasma over the cusp and lobes. In Figure 7b, at 5:26:44 UT, the DF had a parallel velocity and took on a D shape, which is typical of an observation of a reconnection jet [*Cowley*, 1982; *Trattner et al.*, 2012b]. From Figure 3, this distribution was measured during a time when C1 observed a southward/tailward magnetic field vector ($B_L < 0$) and the tailward jet. Figure 7c shows the first time the D-shaped distribution turned from parallel to antiparallel at 5:27:17 UT. This corresponds to the jet reversal in Figure 3. After this point, C1 remained in the sunward exhaust for several minutes, including when the DF in Figure 7d was measured.

The reversal in exhaust direction observed in the C1 DFs should have propagated to C3 if the structure was truly moving tailward and southward. Figure 8 shows ion DFs measured by the HIA instrument on C3, with start times of the measurement interval corresponding to the vertical dashed lines in Figure 6. Figure 8a shows a D-shaped DF with parallel streaming. From Figure 6, the magnetic field is in the tailward/southward direction, as well as the bulk velocity, verifying that C3 was observing a tailward exhaust. Figure 8b shows the first reversal of the exhaust observed by C3, with a D-shaped DF at an antiparallel (sunward and northward) velocity. It should be noted that in the DFs measured during the times between Figures 7b and 7c, as well as between Figures 8a and 8b, there is no evidence of a magnetic island or chain of magnetic islands. Therefore,

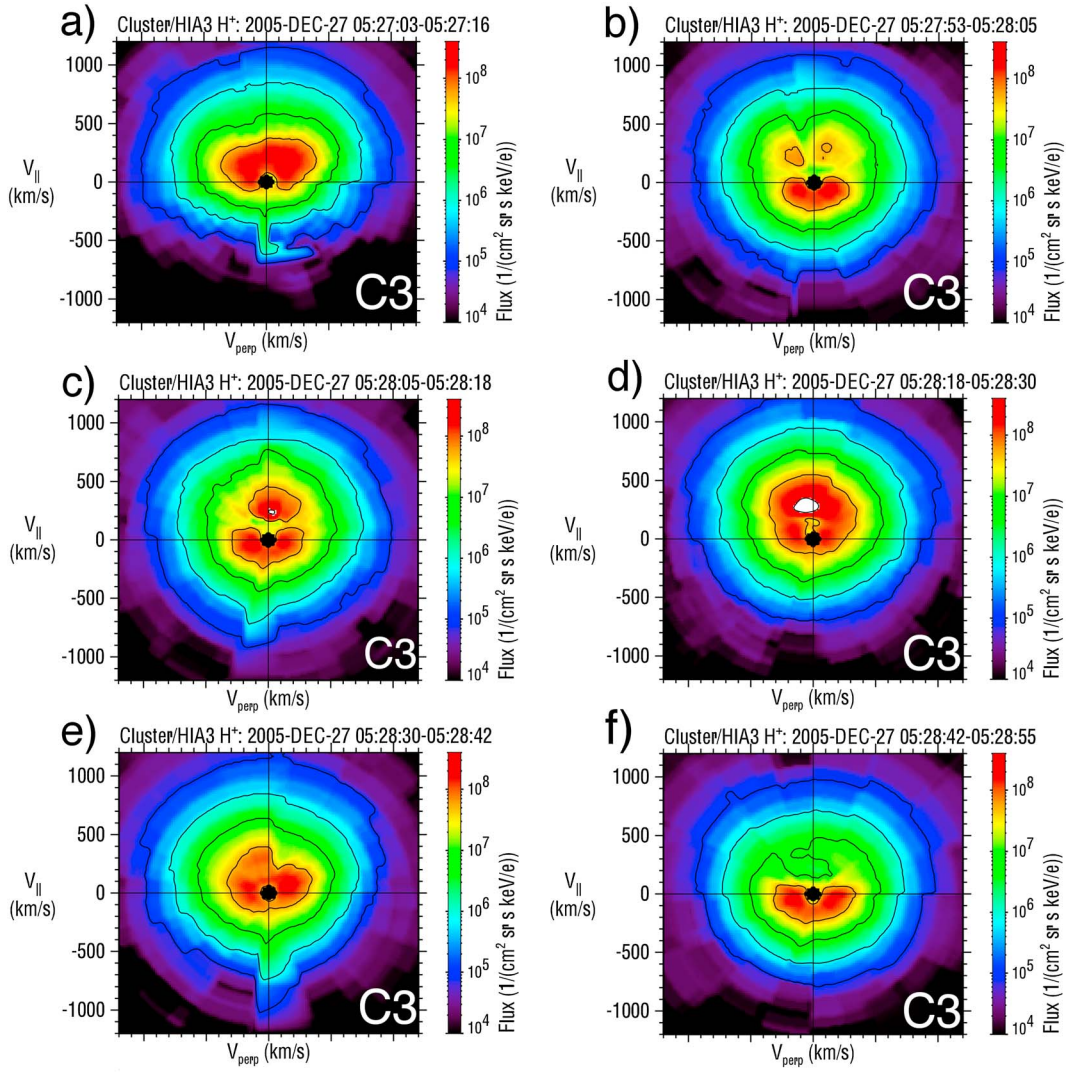

Figure 8. (a–f) Cluster 3 ion distributions in the *X-Z* plane calculated over 13 s intervals with the start times corresponding to the vertical dashed lines in Figure 6.

Figures 7b and 8a are likely showing measurements of the same exhaust. This suggests that the *x* line that passed C1 also passed C3.

If we look at the times at which C1 and C3 first observed the reversal in the reconnection exhaust direction, which were 5:27:17 and 5:27:53 UT, respectively, we can divide by the total separation between the two spacecraft (5535 km) and determine that the *x* line traveled from C1 to C3 at 154 km/s. Because the distribution functions are time averaged, there is a significantly large error introduced into this calculation (e.g., the 12 s averaging mode of C3 can lead to a velocity which could be as small as 117 km/s). Another, more accurate way to calculate the speed of the *x* line retreat is via the Hall field signatures. In Figure 3, when the exhaust turns from tailward to sunward, the perturbation in B_M turns negative, reaching a local minimum inside the exhaust. In Figure 6, the B_M also reaches a local minimum the first time the *L* component of the flow turns sunward. This is more clearly demonstrated in Figure 9, which shows the magnetic field in the GSM coordinates for C1, C3, and C4. From the minimum variance analysis, the *M* component is largely in the Y_{GSM} direction. Using the two local minima highlighted in Figure 9 as another proxy for the jet reversal, we can also approximate the *x* line speed. With the high-resolution FGM data, the time resolution is 0.04 s, and the error due to timing is negligible. Using this method, the time between B_M minima is 40 s, and the total speed of the *x* line is 136 km/s.

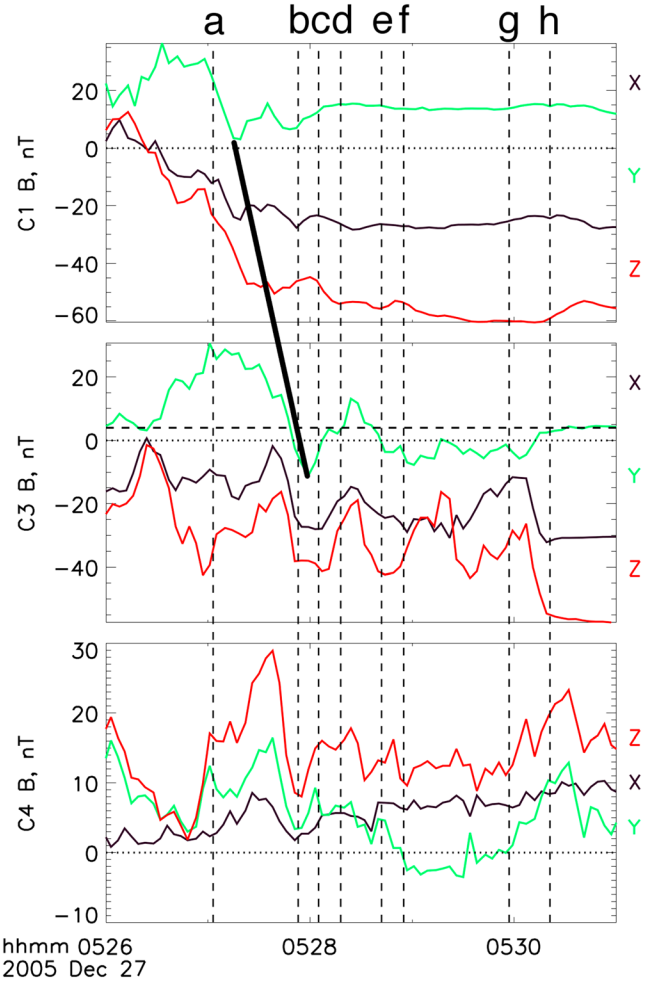

Figure 9. (top to bottom) Clusters 1, 3, and 4 magnetic field data. All three time series are given in geocentric solar magnetospheric (GSM) coordinates. The vertical dashed lines correspond to the ion distributions shown in Figure 8. The diagonal black line shows the two minima in the Hall field signatures that were used to trace the motion of the *x* line.

The velocity of this *x* line retreat in the *X-Z* plane is 105 km/s, while the magnetosheath velocity in the *X-Z* plane is 106 km/s. Alternatively, in the *L* direction, the velocity of the *x* line retreat is −108 km/s, while the magnetosheath velocity in the *L* direction is 104 km/s. This means that the *x* line retreats at approximately the magnetosheath flow speed. One way to understand this is through asymmetric reconnection theory. *Cassak and Shay* [2007, 2009] predicted that in the diffusion region, the *x* line and the flow stagnation point would be offset from each other, with the *x* line offset toward the weak field side and the stagnation point being offset toward the low-density side. Because the density in the magnetosheath is approximately between 60 and 75 cm^{-3} and the density on the magnetospheric side is between 0.1 and 0.5 cm^{-3}, based on equation (27) from *Cassak and Shay* [2007], we expect the stagnation point to be between 500 to 3000 times closer to the magnetospheric side of the dissipation region than to the magnetosheath side. This suggests that the magnetosheath plasma flows nearly all the way across the dissipation region, so it governs the rate of *x* line retreat.

The *x* line moving at the magnetosheath flow speed may appear to contradict the hypothesis that the *x* line motion makes the magnetosheath sub-Alfvénic in the *x* line's own frame [e.g., *Gosling et al*., 1991; *Fuselier et al*., 2000]. The observed motion of the *x* line in the present study simply shifts the flow shear to the magnetospheric side of the current sheet. However, the density on the magnetospheric side is very low (<0.5 cm^{-3}), leading to a local Alfvén speed of at least 1850 km/s. Therefore, even in the frame of the moving *x* line, the magnetospheric plasma is still moving slower than the local Alfvén speed.

3.2. Magnetic Island Formation Tailward of the *X* Line

After C1 observed the flow reversal from the negative *L* direction to positive *L*, it was in the sunward ($V_L > 0$) jet for the remainder of the time period of interest. In terms of the DFs in Figure 7, after the reversal at 5:27:17 UT, C1 continued to see the D-shaped DFs with antiparallel streaming, such as in Figures 7c and 7d. From Figure 8, it is apparent that C3 encountered a more complex structure. For all six DFs, the magnetic field was in the negative *L* direction, and therefore, parallel streaming corresponds to a tailward (−*L*) velocity, and antiparallel streaming corresponds to a sunward (+*L*) velocity. Figures 8a and 8b correspond to the first reversal of the jet. At the time the distribution function in Figure 8c was measured, bidirectional streaming was observed. There are also very low density populations suggesting bidirectional streaming in Figure 8b as well, which may be due to a second *x* line beginning to form between C1 and C3 and will be discussed in further detail in section 3.3. In Figure 8d, C3 observed a filling out of phase space with a bulk velocity that was slightly tailward.

In Figure 8e, the distribution function became complex, again with tailward bulk velocity, followed by another sunward jet in Figure 8f. After Figure 8f, C3 observed filled out phase space again (not shown), and the structure was not as clear.

The counterstreaming ion populations in Figure 8c are indicative of being inside a magnetic island [e.g., *Hasegawa et al*., 2010; *Trattner et al*., 2012a, 2012b]. In order to determine if the counterstreaming population does signify a magnetic island, a few alternative explanations need to be eliminated. For example, from Figure 6 (top), it is apparent that the *L* component of the magnetic field was highly variable during this interval. It is therefore important to verify that C3 did not end up in the magnetosheath after a southward turning of the IMF, which can be done by comparing the magnetic field data on C3, which crossed the magnetopause, with C4, which remained in the magnetosheath during this interval and did not cross the magnetopause until approximately 6:10 UT (not shown).

Figure 9 shows FGM data in the GSM coordinates for C1, C3, and C4 during the same time interval as Figure 6. During this time, C1 saw a rotation from positive to negative in both the *X* and *Z* components of the magnetic field. C3 observed a fluctuating negative field in both the *X* and *Z* components. Finally, C4 observed a fluctuating field with the *X* and *Z* components being positive. Therefore, during the entire interval, C4 was in the magnetosheath, with a northward and sunward field, while C3 observed a field that was southward and tailward, which is typical of lobe field lines poleward of the cusp. It is therefore likely that the structure observed by C3 during the interval is a magnetopause structure and not a magnetosheath one.

Another alternative explanation for a counterstreaming ion population in a high-latitude reconnection exhaust is that it consists of ions that have been reflected from the cusp by the magnetic mirror force [e.g., *Fuselier et al*., 2000; *Trattner et al*., 2007]. The parallel ions observed by C1 in Figure 7d are an example of a reflected population. It is particularly worth noting that the reflected population was less dense and had a faster bulk velocity than the main exhaust due to a time of flight effect where the faster ions can reach the detector from the mirror point first.

To determine whether the counterstreaming populations in Figure 8 are the result of an island or a reflected population, Figure 10 shows the corresponding cuts in the DFs at $V_\perp = 0$. There is evidence of counterstreaming ions in all panels of Figure 10 except Figures 10a and 10e. In all of these panels, with the exception of Figure 10f, the phase-space densities of the two counterstreaming populations were comparable. While it is possible for a mirrored population to be comparable in phase-space density and velocity if the spacecraft remains in a stable structure for a significant amount of time, the structure observed by C1 and C3 was moving fast enough for this to be unlikely. Therefore, it is probable that the counterstreaming populations observed by C3 are indicative of an island.

3.3. Structure of the Island

Figure 11 shows a diagram of a possible expected magnetic field structure for a single magnetic island on the magnetopause boundary. The upper limit on the size of this structure would be the separation between C1 and C3 in the *L* direction, which is 0.69 Re. The out-of-plane fields are determined assuming that the higher-density plasma will contribute to the current loops that generate the Hall fields in the ion diffusion region. The possible positions of the spacecraft along *L* for each panel in Figures 8 and 10 are also labeled and will be discussed in further detail below. To the left and right of the island, we have the magnetic field signature in the sunward and tailward exhausts, respectively, for northward IMF. Inside the island, on the left side, there is a positive (out of the page) Hall field, and one expects a tailward $J \times B$ force and jet. On the right side of the island, there is a negative (into the page) Hall field, and one expects a sunward $J \times B$ force and jet. If an island did form tailward of C1 and encounter C3 as the *x* line retreated, the magnetic field and velocity signatures should be consistent with the diagram in Figure 11.

During the time the distribution in Figure 8a was measured, C3 observed the tailward exhaust, which would be to the right of the island in Figure 11. During this time, there should be a positive deviation from the background guide field in Figure 9. Under the assumption that the *L* direction is in the X-Z_{GSM} plane, and treating the Y_{GSM} direction as out of plane, C3 observed a positive deviation from the background magnetospheric value, implying that the spacecraft was sitting in the tailward exhaust near the ion diffusion region. At the time the distribution in Figure 8b was measured, C3 encountered a sunward exhaust.

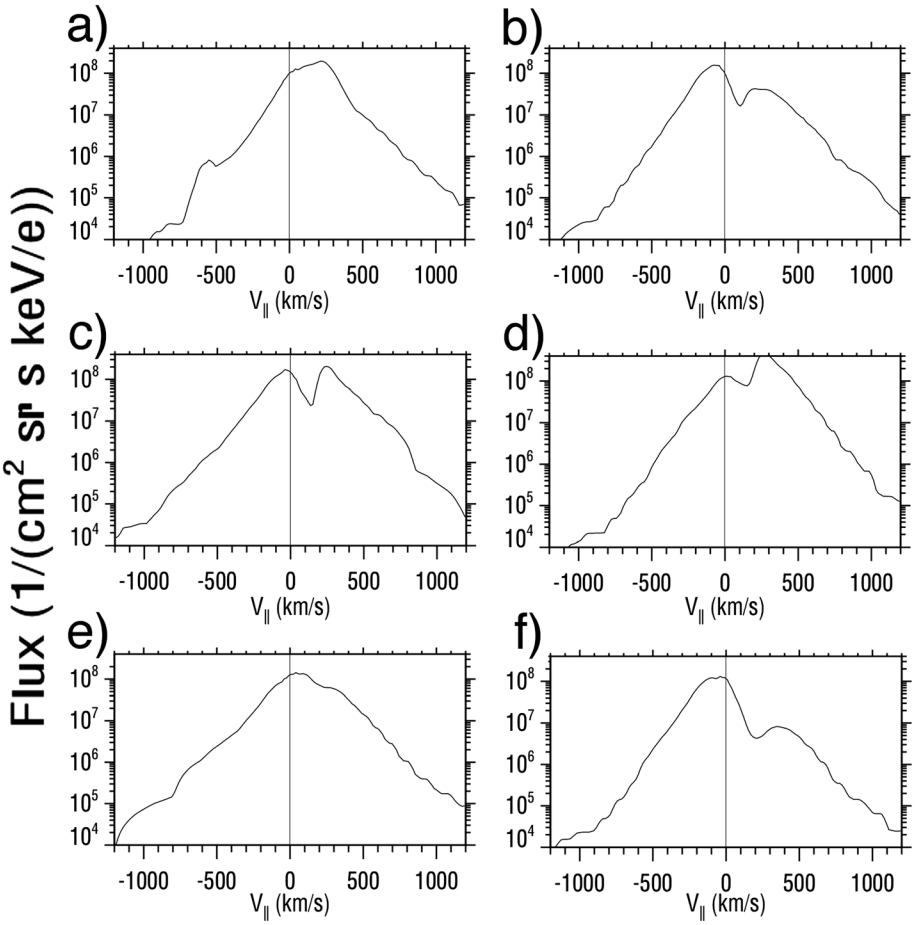

Figure 10. (a–f) Cuts in the Cluster 3 ion distributions from Figure 8 at $V_{\perp} = 0$. The lettering of the panels corresponds directly to the panels in Figure 8.

Additionally, there was a negative deviation of the B_Y component shown in Figure 9. Counter streaming ions with very low phase space density were also observed. In Figure 8c, the bulk velocity was still approximately sunward, and B_Y still had a negative deviation; however, there was strong evidence of a counterstreaming population.

Figures 8b and 8c imply that C3 was in an island but still near the sunward jet region on the right side of the island's center in Figure 11, which in turn implies that a second *x* line was formed between C1 and C3. A possible sequence of events is as follows. (1) C3 was already in the tailward exhaust, and C1 crossed into that exhaust. (2) The *x* line retreated past C1, and the spacecraft observes the sunward exhaust. (3) Shortly after, C3 also crossed into the sunward exhaust. (4) Sometime between (2) and (3), a second *x* line formed between C1 and C3, with C1 remaining in the sunward exhaust and C3 in a magnetic island.

In Figure 8d, phase space filled out, and the bulk velocity turned tailward again. In Figure 10d, there are two peaks in the distribution function, indicating counterstreaming populations, but the parallel (tailward) stream dominates. From Figure 9, the B_Y component returned to the background level, which implies that C3 was in the center of an island traveling tailward, skewed slightly toward the tailward jet side. Shortly after, around the time Figure 8e was measured, the velocity moment reached a minimum in the negative *L* direction as seen in Figure 6. At this time, the B_Y component had a positive deviation, implying that the spacecraft had encountered the left-hand side of the island such as in the diagram in Figure 11, with a tailward exhaust. In Figure 8f, the velocity turned sunward again, and negative perturbations in B_Y were observed, which implied an encounter of a sunward exhaust near the ion diffusion region. Additionally, there was some evidence of counterstreaming ions; however, the density of parallel streaming ions was much smaller. After the distribution in Figure 8f was observed, C3

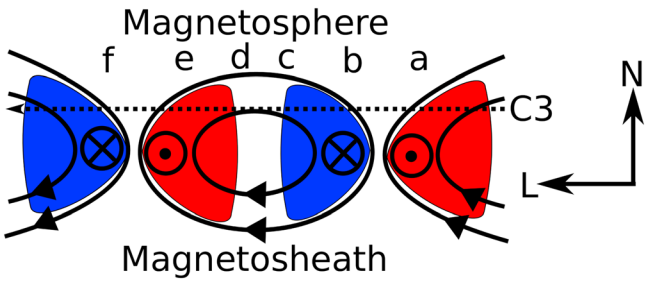

Figure 11. Diagram of the expected structure of a single magnetic island under the assumption that the higher density plasma governs the Hall field orientation. The red and blue regions indicate the possible location of positive and negative Hall fields, respectively. The arrows correspond to the magnetic field direction. It should be noted that the distortion of the in-plane magnetic field due to magnetic field and density asymmetries across the current sheet are not included in this figure and would likely lead to a more dominant *L* component on the magnetospheric side. The dashed line corresponds to the trajectory of the C3 spacecraft in the frame of the moving island and *x* lines.

continued to observe filled-out phase space such as in Figure 8d until the observation of the sunward jet at approximately 5:31 UT (not shown). It is unclear what sort of structure passed the spacecraft at this time, especially since from Figure 9, the spacecraft was observing magnetospheric or boundary layer magnetic field signatures. It is possible that other phenomena, such as Kelvin–Helmholz instabilities, could be leading to a highly complicated structure that is difficult to resolve given the temporal and spatial resolution of the instruments. Inward and outward motions of the magnetopause boundary are also a possibility.

4. Summary and Conclusion

In the present study, an event during northward IMF conditions where two Cluster spacecraft crossed a reconnection *x* line region was investigated. Because both spacecraft observed jet reversals, and comparable Hall field signatures, we were able to directly measure the speed at which the *x* line moved, as opposed to finding the deHoffmann–Teller speed and assuming it as a proxy for *x* line motion. As far as we know, this is the first study to do this. We found that the *x* line retreated tailward at a velocity comparable to the magnetosheath speed. This is consistent with the current understanding of asymmetric reconnection, especially the idea that the stagnation point is offset toward the low-density side, while the *x* line is offset to the low-magnetic field side of the dissipation region [*Cassak and Shay*, 2007, 2009]. The results are also consistent with the idea that the flow shear becomes sub-Alfvenic in the reference frame of the moving *x* line [*Gosling et al*., 1991; *Fuselier et al*., 2000].

Additionally, we observed the formation of a second *x* line between the two Cluster spacecraft, leading to a tailward propagating magnetic island. This included observations of both Hall magnetic field signatures and counterstreaming ion distribution functions consistent with a magnetic island. The formation of multiple retreating *x* lines and magnetic islands in response to a super-Alfvénic magnetosheath flow during high-latitude reconnection intervals is consistent with the observations and conclusions made by *Hasegawa et al*. [2008]. The present study provides additional support of their argument due to the close proximity of the two Cluster spacecraft to the *x* line, as verified by the Hall field signatures. Additionally, given the short time frame of the study, multiple *x* lines may form to replace those that retreat on the order of only a few minutes. It is also worth noting that despite conditions where islands can form, both exhausts observed by C1 passed the Walén test. This implies that the island formed far enough down tail from C1 to not violate the assumption of a rotational discontinuity but still somewhere between C1 and C3.

One reason that the *x* line is unstable could be the unusually fast magnetosheath flow in the event studied. The average sheath conditions observed by Cluster prior to the magnetopause crossing included a bulk flow speed of 139.7 km/s and an Alfvén speed of 61.3 km/s, giving an Alfvénic Mach number of 2.3. While the super-Alfvénic magnetosheath flow does not appear to suppress reconnection, it does seem to lead to a highly unstable configuration, where the *x* line retreats tailward as soon as it is formed, followed by the formation of a second *x* line.

Another significant result is the lack of observed electron heating above the magnetosheath background energy spectrum as either spacecraft crossed the magnetopause. This is consistent with the hypothesis that the observation of electron heating caused by reconnection involves a time-of-flight effect and therefore will not occur close to the diffusion region [*Fuselier et al*., 2012].

Although generally considered geomagnetically "quiet," intervals where the IMF is northward and reconnection can occur poleward of the cusp, are still highly dynamic. Additionally, magnetic reconnection during these intervals can have strong localized impacts on the polar ionosphere-thermosphere system [*Eriksson et al*., 2005; *Wilder et al*., 2011, 2012]. One of the major challenges in predicting the system-wide effects is predicting when and how magnetic reconnection occurs at high latitudes poleward of the cusp, and the problem of reconnection under high-flow shear conditions exacerbates this challenge. A better understanding of both *x* line retreat and the formation of multiple islands will assist in better understanding the system as a whole. There are several unresolved questions that remain. For example, how far will a single *x* line retreat before a new one forms? What conditions govern the formation of the second *x* line? Does the *x* line always retreat at the speed of the magnetosheath flow especially under strong IMF conditions where the *x* line may not be offset as close to the magnetosheath? Is there a way to predict the *x* line retreat speed using magnetosheath conditions? Further work is needed to better understand these dynamics.

Acknowledgments

F.D.W. is supported by NSF GEM grant AGS-1303649. S.E. is supported by NASA grant NNX10AQ45G. K.J.T. is supported by NASA grant NNX08AF35G and by the NSF under grant 1102572. P.A.C. is supported by NSF grant AGS-0953463. Cluster spacecraft data are available via the Cluster Active Archive (http://caa.estec.esa.int/). The authors acknowledge helpful discussions on the retreat speed with C.E. Doss and C.M. Komar. We also acknowledge useful feedback from T.D. Phan during the early stages of this study.

Yuming Wang thanks Xu-Zhi Zhou and another reviewer for their assistance in evaluating this paper.

References

Balogh, A., et al. (2001), The Cluster magnetic field investigation: Overview of in-flight performance and initial results, *Ann. Geophys.*, *19*, 1207–1217.

Cassak, P. A., and M. A. Shay (2007), Scaling of asymmetric magnetic reconnection: General theory and collisional simulations, *Phys. Plasmas*, *14*, 102114, doi:10.1063/1.2795630.

Cassak, P. A. and M. A. Shay (2009), Structure of the dissipation region in fluid simulations of asymmetric magnetic reconnection, *Phys. Plasmas*, *16*, 055704, doi:10.1063/1.3086867.

Cowley, S. W. H. (1982), The cause of convection in the Earth's magnetosphere: A review of developments during the IMS, *Rev. Geophys.*, *20*, 531–565, doi:10.1029/RG020i003p00531.

Crooker, N. (1992), Reverse Convection, *J. Geophys. Res.*, *97*, 19,363–19,372, doi:10.1029/92JA01532.

Dungey, J. (1963), The structure of the exosphere or adventures in velocity space, in *Geophysics, The Earth's Environment*, edited by C. DeWitt, J. Hieblot, and A. Lebeau, pp. 505, Gordon and Breach, New York.

Dungey, J. W. (1961), Interplanetary magnetic field and the auroral zones, *Phys. Rev. Lett.*, *6*, 47–48.

Eriksson, S., et al. (2004), Global control of merging by the interplanetary magnetic field: Cluster observations of dawnside flank magnetopause reconnection, *J. Geophys. Res.*, *109*, A12203, doi:10.1029/2003JA010346.

Eriksson, S., et al. (2005), On the generation of enhanced sunward convection and transpolar aurora in the high latitude ionosphere by magnetic merging, *J. Geophys. Res.*, *110*, A11218, doi:10.1029/2005JA011149.

Escoubet, C. P., M. Fehringer, and M. Goldstein (2001), The Cluster mission, *Ann. Geophys.*, *19*, 1997–1200.

Fuselier, S. A., S. M. Petrinec, and K. J. Trattner (2000), Stability of the high-latitude reconnection site for steady northward IMF, *Geophys. Res. Lett.*, *27*, 473–476, doi:10.1029/1999GL003706.

Fuselier, S. A., K. J. Trattner, and S. M. Petrinec (2011), Antiparallel and component reconnection at the dayside magnetopause, *J. Geophys. Res.*, *116*, A10227, doi:10.1029/2011JA016888.

Fuselier, S. A., K. J. Trattner, S. M. Petrinec, and B. Lavraud (2012), Dayside magnetic topology at the Earth's magnetopause for northward IMF, *J. Geophys. Res.*, *117*, A08235, doi:10.1029/2012JA017852.

Gosling, J. T., M. F. Thomsen, S. J. Bame, R. C. Elphic, and C. T. Russel (1991), Observations of reconnection of interplanetary and lobe magnetic field lines at the high-latitude magnetopause, *J. Geophys. Res.*, *96*, 14,097–14,106, doi:10.1029/91JA01139.

Hasegawa, H., A. Retinó, A. Vaivads, Y. Khotyaintsev, R. Nakamura, T. Takada, Y. Miyashita, H. Réme, and E. A. Lucek (2008), Retreat and reformation of X-line during quasi-continuous tailward-of-the-cusp reconnection under northward IMF, *Geophys. Res. Lett.*, *35*, L15104, doi:10.1029/2008GL034767.

Hasegawa, H., et al. (2010), Evidence for a flux transfer event generated by multiple X-line reconnection at the magnetopause, *Geophys. Res. Lett.*, *37*, L16101, doi:10.1029/2010GL044219.

Johnstone, A. D., et al. (1997), Peace: A Plasma Electron and Current Experiment, *Space Sci. Rev.*, *79*, 351–398.

Kessel, R. L., S.-H. Chen, J. L. Green, S. F. Fung, S. A. Boardsen, L. C. Tan, T. E. Eastman, J. D. Craven, and L. A. Frank (1996), Evidence of high-latitude reconnection during northward IMF: Hawkeye observations, *Geophys. Res. Lett.*, *23*, 583–586, doi:10.1029/95GL03083.

Lepping, R. P., et al. (1995), The Wind magnetic field investigation, *Space Sci. Rev.*, *71*, 207–229.

Lin, R. P., et al. (1995), A three-dimensional plasma and energetic particle investigation for the Wind spacecraft, *Space Sci. Rev.*, *71*, 125–153.

Lybekk, B., A. Pedersen, S. Haaland, K. Svenes, A. N. Fazakerley, A. Masson, M. G. G. T. Taylor, and J.-G. Trotignon (2012), Solar cycle variations of the Cluster spacecraft potential and its use for electron density estimations, *J. Geophys. Res.*, *117*, A01217, doi:10.1029/2011JA016969.

Malakit, K., M. A. Shay, P. A. Cassak, and C. Bard (2010), Scaling of asymmetric magnetic reconnection: Kinetic particle-in-cell simulations, *J. Geophys. Res.*, *115*, A10223, doi:10.1029/2010JA015452.

Mozer, F. S., V. Angelopoulos, J. Bonnell, K. H. Glassmeier, and J. P. McFadden (2008a), THEMIS observations of modified Hall fields in asymmetric magnetic field reconnection, *Geophys. Res. Lett.*, *35*, L17S04, doi:10.1029/2007GL033033.

Mozer, F. S., P. L. Pritchett, J. Bonnell, D. Sundkvist, and M. T. Chang (2008b), Observations and simulations of asymmetric magnetic field reconnection, *J. Geophys. Res.*, *113*, A00C03, doi:10.1029/2008JA013535.

Paschmann, G., B. U. Ö. Sonnerup, I. Papamastorakis, N. Sckopke, G. Haerendel, S. J. Bame, J. R. Asbridge, J. T. Gosling, C. T. Russel, and R. C. Elphic (1979), Plasma acceleration at the earth's magnetopause: Evidence for magnetic reconnection, *Nature*, *282*, 243.

Phan, T., et al. (2003), Simultaneous Cluster and IMAGE observations of cusp reconnection and auroral proton spot for northward IMF, *Geophys. Res. Lett.*, *30*(10), 1509, doi:10.1029/2003GL016885.

Phan, T. D., B. U. Ö. Sonnerup, and R. P. Lin (2001), Fluid and kinetics signatures of reconnection at the dawn tail magnetopause: Wind observations, *J. Geophys. Res.*, *106*, 25,489–25,501, doi:10.1029/2001JA900054.

Phan, T. D., et al. (2004), Cluster observations of continuous reconnection at the magnetopause under steady interplanetary magnetic field conditions, *Ann. Geophys.*, *22*, 2355–2367.

Rème, H., et al. (2001), First multipspacecraft ion measurements in and near the Earth's magnetosphere with the identical Cluster ion spectrometry (CIS) experiment, *Ann. Geophys.*, *19*, 1303–1354.

Sonnerup, B. U. Ö. (1971), Magnetopause structure during the magnetic storm of September 24, 1961, *J. Geophys. Res.*, *76*, 6717–6735, doi:10.1029/JA076i028p06717.

Sonnerup, B. U. Ö., and M. Scheible (1998), Minimum and maximum variance analysis, in *Analysis Methods for Multi-Spacecraft Data*, ISSI Sci. Rep., *SR-001*, edited by G. Paschmann and P. W. Daly, p. 185–220, ESA Publ. Div., Noordwijk, Netherlands.

Sonnerup, B. U. Ö., G. Paschmann, I. Papamastorakis, N. Sckopke, G. Haerendel, S. J. Bame, J. R. Asbridge, J. T. Gosling, and C. T. Russell (1981), Evidence for magnetic field reconnection at the Earth's magnetopause, *J. Geophys. Res.*, *86*, 10,049–10,067, doi:10.1029/JA086iA12p10049.

Sonnerup, B. U. Ö., I. Papamastorakis, G. Paschmann, and H. Lühr (1987), Magnetopause properties from AMPTE/IRM observations of the convection electric field: Method development, *J. Geophys. Res.*, *92*, 12,137–12,159, doi:10.1029/JA092iA11p12137.

Sonnerup, B. U., I. Papamastorakis, G. Paschmann, and H. Lühr (1990), The magnetopause for large magnetic shear: Analysis of convection electric fields from AMPTE/IRM, *J. Geophys. Res.*, *95*(A7), 10,541–10,557, doi:10.1029/JA095iA07p10541.

Trattner, K. J., J. S. Mulcock, S. M. Petrinec, and S. A. Fuslier (2007), Probing the boundary between antiparallel and component reconnection during southward interplanetary magnetic field conditions, *J. Geophys. Res.*, *112*, A08210, doi:10.1029/2007JA012270.

Trattner, K. J., S. M. Petrinec, S. A. Fuselier, and T. D. Phan (2012a), The Location of the Reconnection Line: Testing the Maximum Magnetic Shear Model with THEMIS observations, *J. Geophys. Res.*, *117*, A01201, doi:10.1029/2011JA016959.

Trattner, K. J., S. M. Petrinec, S. A. Fuselier, N. Omidi, and D. G. Sibeck (2012b), Evidence of multiple reconnection lines at the magnetopause from cusp observations, *J. Geophys. Res.*, *117*, A01213, doi:10.1029/2011JA017080.

Trenchi, L., M. F. Marcucci, G. Pallocchia, G. Consolini, M. B. Bavassano Cattaneo, A. M. Di Lellis, H. Reme, L. Kistler, C. M. Carr, and J. B. Cao (2008), Occurrence of reconnection jets at the dayside magnetopause: Double Star observations, *J. Geophys. Res.*, *113*, A07S10, doi:10.1029/2007JA012774.

Wilder, F. D., C. R. Clauer, J. B. H. Baker, and P. T. Newell (2011), Inter-hemispheric observations of dayside convection under northward IMF, *J. Geophys. Res.*, *115*, A10230, doi:10.1029/2011JA016748.

Wilder, F. D., G. Crowley, S. Eriksson, P. T. Newell, and M. R. Hairston (2012), Ionospheric Joule heating, fast flow channels, and magnetic field line topology for IMF By-dominant conditions – Observations and comparisons with predicted reconnection jet speeds, *J. Geophys. Res.*, *117*, A11311, doi:10.1029/2012JA017914.